Vpliv troposferskega modeliranja in atmosferskega tlaka na ponovljivost položaja GNSS

Impact of tropospheric modelling and atmospheric pressure loading on GNSS position repeatability

Hicham Dekkiche, Houaria Namaoui, Walid Bouaoula, Yasser Bedjaoui, Karim Bensttila

UDK: 528.835:629.056.8(100)
Klasifikacija prispevka po COBISS.SI: 1.01
Prispelo: 27. 2. 2025
Sprejeto: 7. 9. 2025

DOI: doi.org/10.15292/geodetski-vestnik.2025.04.554-573
SCIENTIFIC ARTICLE
Received: 27. 2. 2025
Accepted: 7. 9. 2025

IZVLEČEK

Študija preučuje vpliv strategij modeliranja troposfere na ponovljivost dnevnih ocen položaja GNSS v sredozemskih in visokogorskih regijah na podlagi celovite analize več dejavnikov: ocene skupne zakasnitve v zenitu, mejnih kotov višine (0°, 3° in 7°), projekcijske komponente troposferske refrakcije (VMF1, NMF, GMF) in popravkov atmosferskega tlaka. Raziskava kaže, da ocena parametrov skupne zakasnitve v zenitu skupaj z vodoravnimi gradienti znatno izboljša ponovljivost položaja, saj zmanjša napake vertikalne komponente z več kot enega metra na milimetrske ravni. Izbor kota odklopa višine prav tako vpliva na zmogljivost, pri čemer 3° daje optimalne rezultate, medtem ko jih 0° dosledno poslabšuje. Učinkovitost kartografske funkcije se razlikuje glede na regijo: v Sredozemlju NMF nekoliko prekaša druge v navpični smeri, medtem ko VMF1 in NMF izstopata v vodoravni smeri; v regijah z visoko zemljepisno širino GMF na splošno deluje najbolje, čeprav obstaja odvisnost od postaje. Vključitev popravkov za atmosferski tlak rezultate večinoma izboljša, zlasti pri uporabi z VMF1, ki je pokazal do 12-odstotno izboljšanje vertikalne ponovljivosti. Te ugotovitve poudarjajo prednosti integriranega pristopa, ki združuje napredne funkcije kartiranja z atmosferskimi popravki.

KLJUČNE BESEDE

modeliranje troposfere, obremenitev z atmosferskim tlakom, GNSS-pozicioniranje, dnevna ponovljivost

ABSTRACT

This study investigates the impact of tropospheric modelling strategies on the repeatability of daily GNSS position estimates across Mediterranean and high-latitude regions through comprehensive analysis of multiple factors: zenith total delay estimation, elevation cut-off angles (0°, 3° and 7°), mapping functions (VMF1, NMF, GMF), and atmospheric pressure loading corrections. The research demonstrates that estimating zenith total delay parameters alongside horizontal gradients substantially improves position repeatability, reducing vertical component errors from over one meter to millimetric levels. The choice of elevation cut-off angle also affects performance, with 3° yielding optimal results, while 0° consistently degrades it. Mapping function effectiveness varies by region: in the Mediterranean, NMF slightly outperforms others vertically, whereas VMF1 and NMF excel horizontally; in high-latitude regions, GMF generally performs best, though station-dependent variability persists. Incorporating atmospheric pressure loading corrections improves results in most cases, especially when used with VMF1, which showed up to 12% improvement in vertical repeatability. These findings underscore the benefits of an integrated approach combining advanced mapping functions with atmospheric corrections.

KEY WORDS

Troposphere modelling, Atmospheric pressure loading, GNSS positioning, daily repeatability

1 INTRODUCTION

Global Navigation Satellite Systems (GNSS) play a critical role in high-accuracy positioning applications, including geodesy, geodynamics and environmental monitoring. The accuracy of GNSS solutions is particularly crucial for long-baseline differential positioning, where errors caused by atmospheric effects are no longer correlated and considerably degrade the GNSS performance. Among these, tropospheric delay and ATMospheric pressure Loading (ATML) are challenging contributors to positioning errors that are difficult to manage.

The tropospheric delay is frequency-independent and cannot be mitigated by dual-frequency observations; its impact depends on temperature, pressure, and water vapour content, which exhibit significant spatial inhomogeneity and temporal variability (Torres et al., 2010; Van Malderen et al., 2014; Namaoui, 2022). Its magnitude varies significantly with elevation angle, ranging from approximately 2.0 to 2.6 meters in the zenith direction to 20-28 meters near the horizon at lower elevation angles (El-Rabbany, 2002). This elevation-dependent behaviour necessitates the use of mapping functions to project zenith delays to arbitrary elevation angles. Accurate modelling of tropospheric delay is thus essential for applications requiring sub-centimetre precision.

The development of tropospheric delay models has evolved significantly over the past decades. Early models such as the (Hopfield, 1969) and (Saastamoinen, 1972) provided fundamental frameworks but showed limitations in accuracy. The Niell Mapping Function (NMF) introduced by (Niell, 1996) marked a significant advancement, providing latitude and day-of-year dependent mapping functions that improved delay-modelling accuracy, particularly for mid-latitude regions. The Vienna Mapping Function (VMF) concept, introduced by (Böhm et al., 2006a), utilizes numerical weather model data to provide site-specific and time-dependent mapping functions, representing a paradigm shift from empirical models to physics-based modelling. The Global Mapping Function (GMF) developed by (Böhm et al., 2006b) offers a compromise between accuracy and computational efficiency, providing improved performance over NMF while maintaining broader applicability without requiring real-time meteorological data.

Several studies have investigated the impact of tropospheric mapping functions on the accuracy of geodetic coordinate estimates (Tesmer et al., 2007; Urquhart et al., 2014; Landskron & Böhm, 2018). These studies demonstrate that while improvements in tropospheric mapping functions yield incremental gains in geodetic accuracy, especially at low elevation angles and in challenging environments, the choice of model should consider site characteristics, available meteorological data, and computational resources. They also show that, typically, improvements in coordinate repeatability are not consistent across all stations.

In addition to tropospheric delay, atmospheric pressure loading, although less influential, still introduces systematic errors in GNSS positioning. The concept involves the response of the solid Earth to spatially and temporally varying atmospheric pressure loads. Soil displacements can reach up to ±2.5 cm in the vertical component and ±0.25 cm in horizontal components (Rabbel & Zschau, 1985; Luo, 2001).

Studies investigating the impact of atmospheric pressure loading on geodetic coordinate estimates such as those performed by (van Dam et al., 1994; Petrov & Boy, 2004; Tregoning & van Dam, 2005; Dach et al.,

2011), highlight that even after applying atmospheric loading corrections, residuals remain significant at specific stations, particularly those in coastal or mountainous regions. These corrections, while beneficial in some cases, do not systematically enhance the geodetic time series or global reference frame solutions.

Theses previous studies have focused on individual error sources in isolation, with limited investigation of the combined impact of tropospheric delay modelling choices and ATML corrections on positioning repeatability. Additionally, comprehensive comparative analysis across diverse geographical settings within a single study framework is lacking, limiting the ability to develop generalized recommendations for optimal model selection.

This study addresses these research gaps by providing the first comprehensive assessment of tropospheric delay mapping function performance specifically tailored to Mediterranean and northern high-latitude regions. Unlike previous studies that examined individual error sources in isolation, this research investigates the combined impact of tropospheric delay modelling using three mapping functions (NMF, VMF1, and GMF) and ATML corrections on positioning repeatability. The study incorporates stations across different latitudinal bands and climatic conditions, enabling robust comparative analysis of mapping function performance across diverse atmospheric regimes.

To achieve our objectives, we process GNSS data using the GAMIT/GLOBK software. This involves analysing 15 days of continuous observations from the Arzew/Algeria GNSS station "ARZE" and eighteen IGS (International GNSS Service) stations located in Mediterranean (mid-latitude) and northern high-latitude regions. The analysis focuses on coordinate repeatability as the primary performance metric, recognising that consistent positioning accuracy is often more important than absolute accuracy for many geodetic applications. The primary objective is to assess the impact of ATML corrections and the three mapping functions on GNSS positioning repeatability. This aims to identify optimal correction strategies and formulate region-specific recommendations for operational GNSS processing within the studied areas.

2 TROPOSPHERIC DELAY AND MAPPING FUNCTIONS

The troposphere is the lower part of the neutral atmosphere, extending from the Earth's surface up to an altitude of about 16 km at the equator and 8 km at the poles. It consists of dry gases and water vapour (Kos et al., 2009).

It accounts for 75 to 80% of the atmospheric mass and contains nearly all the water vapour. The tropospheric delay is influenced by various factors, such as the station's altitude, signal direction, angle of incidence, as well as atmospheric pressure, temperature, and humidity.

Unlike the ionospheric delay, the tropospheric delay d_{trop} cannot be modelled simply by combining signal frequencies. It needs to be considered during the analysis to improve the quality of GNSS positioning. The path can be determined from the refractive index (n), which is commonly expressed in terms of refractivity (N) **(Bevis et al., 1994).**

$$d_{trop} = \int (n - 1) ds \tag{1}$$

$$d_{trop} = 10^{-6} \int N_{trop} ds \tag{2}$$

$$N = 10^6(n-1) = k_1 P_d / T + k_2 P_w / T + k_3 P_w / T^2 \quad (3)$$

Where P_d, T and P_w are respectively the partial pressure of dry air, temperature, and partial pressure of water vapour. **(Thayer, 1974).** k_1, k_2 and k_3 are coefficients of refractivity .

$k_1 = (77.604 \pm 0.04) K / mbar$, $k_2 = (64.79 \pm 0.08) K / mbar$ and $k_3 = (3.776 \pm 0.004) \times 10^5 K^2 mbar$

The tropospheric effect on GNSS is theoretically divided into two components: dry (or hydrostatic) and wet. Thus, the total delays encountered in the troposphere are segmented accordingly.

The dry component, which can reach up to 2.3 m at zenith, can be accurately estimated from the surface pressure and the variation of the gravity field with respect to the latitude and the height above the geoïd (in kilometres) (Saastamoinen, 1972; Davis et al., 1985).

In contrast, the wet component, which can reach up to 50 cm at zenith, is subject to significant spatio-temporal variability based on temperature and humidity (Fernandes et al., 2015, Fernandes and Lázaro, 2016). For this reason, it is often modelled as an unknown parameter that varies over time during the estimation procedure. This tropospheric delay can be divided into two components (d_{wet} wet delay and d_{dry} dry delay)

$$d_{trop} = d_{wet} + d_{dry} \quad (4)$$

To avoid an overly parameterised system, a single parameter ZTD is estimated for a given station and a specific time interval or using a stochastic process. This parameter characterises the tropospheric delay in the zenith direction and assumes a symmetrical distribution of water vapour around the station. However, this assumption is often incorrect, introducing first-order asymmetry, which is corrected by estimating tropospheric horizontal gradients along with other parameters of the state vector.

Tropospheric delay is strongly dependent on satellite elevation. To model this dependence, mapping functions are used. Since the 1970s, many mapping functions have been developed, all of which are representative of a horizontally stratified atmosphere, where the refractive index depends only on the altitude and the distance joining the satellite to the receiver in a vertical plane.

Several studies have been conducted to examine the impact of different mapping functions on GNSS positioning accuracy. Differences in height component can achieve 1 cm by using the NMF and VMF1 (Böhm et al., 2007). Tuka & El-Mowafy (2013) hypothesised that the differences between the mapping functions (MFs) are smaller in the Northern Hemisphere, with VMF1 providing the best results. For the north and east offsets, these mapping functions demonstrated the same level of accuracy. However, for the vertical offsets, VMF1 achieved better accuracy than GMF and NMF, being more consistent with GMF than with NMF (Makabayi & Hunegnaw, 2015).

2.1 Niell Mapping Function

The Niell Mapping Function models the tropospheric delay by mapping the zenith delay to a given elevation angle using a continued fraction form, that is expressed for both wet and hydrostatic components as follows (Niell, 1996):

$$M_i(e) = \frac{1 + \dfrac{a_i}{1 + \dfrac{b_i}{1 + c_i}}}{\sin(e) + \dfrac{a_i}{\sin(e) + \dfrac{b_i}{\sin(e) + c_i}}} \tag{5}$$

Where i = w (wet) or h (hydrostatic), e is the elevation angle, and $a_i b_i$, and c_i are coefficients specific to either the hydrostatic or wet component. In addition to the continued fraction form of the mapping function equation, the NMF hydrostatic component includes a height correction term. Therefore, its final form is expressed as follows:

$$Mf_h = M^h(e) + H \cdot [\frac{1}{\sin(e)} - M_{ht}(e)] \tag{6}$$

H is the height of the site (km), e is the elevation angle, M_{ht} is the continued fraction mapping function at station height.

The coefficients *a*, *b* and *c* in the NMF are determined differently for the hydrostatic, wet, and height correction terms, though all use the same continued fraction form. For the hydrostatic component, the coefficients are calculated by interpolating both average and seasonal amplitude values from tables provided at 15-degree latitude intervals. The final value for each coefficient at a specific site and day of year is obtained by applying a seasonal correction to the interpolated values, using the equation:

$$a = a_{avg} + a_{amp} \cdot \cos\left(\frac{DOY - 28}{365.25} 2\pi\right) \tag{7}$$

Where DOY is the day of year (DOY = 28 for northern hemisphere), a_{avg} and a_{amp} are the average and seasonal amplitude values which can be obtained by the linear interpolation between the nearest latitudes. The similar procedure is applicable to b and c.

In contrast, the coefficients for the wet component depend only on latitude and are interpolated from tabulated average values at 15-degree intervals, with no seasonal or temporal correction applied. For the height correction term in the dry mapping function, a separate set of coefficients is used; these were determined by Niell (1996) through a least-squares fit to the height correction at several elevation angles and are treated as fixed constants, independent of latitude or time.

2.2 Vienna Mapping Function

Although the Vienna Mapping Function uses the same mathematical structure as NMF (eq 5) for both the hydrostatic and wet components, the coefficients *a*, *b* and *c* are different for each component because they are derived from distinct atmospheric properties (Böhm et al., 2006b). For the hydrostatic (dry) component, the coefficients are:

a_h: calculated by ray tracing through the pressure and temperature fields of a numerical weather model (NWM),

b_h and c_h: set to fixed, empirically derived values.

For the wet component, the coefficients are:

a_w: Calculated by ray-tracing through the water vapour field of the NWM,

b_w and c_w: Set to fixed empirical values, which are different from those used for the hydrostatic component.

2.3 Global Mapping Function

The Global Mapping Function is an empirical tropospheric mapping function that has been developed as an improvement on the NMF. Like VMF1, GMF uses the same continued fraction formula (eq 5), but coefficients are derived differently (Böhm et al., 2006b; Böhm et al., 2007). Although the a-coefficient in GMF is modelled using the same functional form as NMF's a-coefficient (eq. 7) its mean value a_{avg} and annual amplitude a_{amp} computation is entirely different, both being obtained from a global fit to multi-year ECMWF Numerical Weather Model (NWM) data using spherical harmonic expansions to degree and order 9 :

$$a_{avg}(\phi,\lambda) = \sum_{n=0}^{9}\sum_{m=0}^{n}\left[C_{nm}\cos(m\lambda) + D_{nm}\sin(m\lambda)\right]P_{nm}(\sin\phi) \tag{8}$$

$$a_{amp}(\phi,\lambda) = \sum_{n=0}^{9}\sum_{m=0}^{n}\left[E_{nm}\cos(m\lambda) + F_{nm}\sin(m\lambda)\right]P_{nm}(\sin\phi) \tag{9}$$

Where the normalized are associated Legendre functions, and C_{nm}, D_{nm}, E_{nm}, F_{nm} are the fitted spherical harmonic coefficients. The b and c coefficients in GMF are set as fixed empirical values.

3 MODELLING OF ATMOSPHERIC PRESSURE LOADING EFFECT

Atmospheric loading models describe the displacements of the Earth's surface caused by variations in atmospheric masses over time. According to **van Dam et al., (1994),** these loads can become significant enough to cause observable deformations. In comparison to methods that do not take this effect into account, their research showed that introducing a correction for atmospheric loads during GNSS data processing improves the repeatability of weekly solutions by up to 20%.

Several meteorological models developed by various research centres, including NCEP, NCAR, ECMWF, and GPT, are essential for estimating this impact. According to the study conducted by (Böhm and Schuh, 2013), two modelling approaches exist, and the RMS (Root Mean Square) difference among 914 GPS stations worldwide is 0.45 mm.

The deformation caused by atmospheric loads primarily results from environmental changes in air masses, which can be equated to variations in water mass. Thus, it is possible to convert daily atmospheric mass loading into an equivalent water height based on the following relationship: "1 Pa corresponds to 0.10197 mm" (Caiya et al., 2020). This approach involves expressing the deformations caused by atmospheric loads as a difference in equivalent water height between a reference value and the study period. The equivalent water height is given by the following relationship: (Caiya et al., 2020)

$$\Delta h(\varphi,\lambda) = R\sum_{n=1}^{N}\sum_{m=0}^{n}[\Delta\overline{C_{nm}^{q}}\cos m\lambda + \overline{\Delta S_{nm}^{q}}\sin m\lambda]\overline{P_{nm}}(\sin\varphi) \tag{10}$$

$$\Delta u(\varphi,\lambda) = 3\frac{\rho_W}{\rho_e}\frac{GM}{\gamma R}\sum_{n=1}^{N}\frac{h_n^{'}}{2n+1}\sum_{m=0}^{n}[\overline{\Delta C_{nm}^{q}}\cos m\lambda + \overline{\Delta S_{nm}^{q}}\sin m\lambda]\overline{P_{nm}}(\sin\varphi) \tag{11}$$

$$\Delta e(\varphi,\lambda) = 3\frac{k_n^{'}\rho_w}{\sin(\varphi)\rho_e}\frac{GM}{\gamma R}\sum_{n=1}^{N}\frac{l_n^{'}}{2n+1}\sum_{m=0}^{n}[\overline{\Delta C_{nm}^{q}}\cos m\lambda + \overline{\Delta S_{nm}^{q}}\sin m\lambda]\frac{\partial}{\partial\lambda}\overline{P_{nm}}(\sin\varphi) \quad (12)$$

$$\Delta n(\varphi,\lambda) = -3\frac{k_n^{'}\rho_w}{\rho_e}\frac{GM}{\gamma R}\sum_{n=1}^{N}\frac{1_n^{'}}{2n+1}\sum_{m=0}^{n}[\overline{\Delta C_{nm}^{q}}\cos m\lambda + \overline{\Delta S_{nm}^{q}}\sin m\lambda]\frac{\partial}{\partial\varphi}\overline{P_{nm}}(\sin\varphi) \quad (13)$$

Δh: The equivalent height of water.

Δu: The displacement along the Up.

Δe: The displacement along the Easting.

Δn: The displacement along the Northing.

φ, λ: The co-latitude and longitude.

ρ_w: The density of water.

ρ_e: The average density of solid earth (5.5×10^3 kg/m^3).

$\overline{P_{nm}}$: The normalised Legendre polynomial.

R: The average radius of the earth.

G: The gravitational constant.

M: The mass of the solid earth.

γ: The average gravity at the surface.

h', k' and l': are the radial, gravity and horizontal Love numbers, respectively.

$\overline{\Delta C_{nm}^{q}}, \overline{\Delta S_{nm}^{q}}$: The variation of the normalised harmonic coefficients of order m and degree n of a period q with respect to a reference period.

In this study, GNSS data were processed using the GAMIT/GLOBK software suite. GAMIT models deformations in three components by convolving surface pressure data with Green's functions, which characterise the Earth's elastic response to point surface loads. The atmospheric pressure inputs are derived from global meteorological models (GPT2), provided as spatio-temporal grids. Both tidal and non-tidal components of atmospheric loading corrections are applied.

4 DATA AND METHODS

4.1 Study area

In this study, a set of eighteen (18) GNSS stations is used. These stations are clustered into two networks located in two different zones: The Mediterranean mid-latitude zone and the high-latitude region. The network in Mediterranean zone is composed of ten (10) stations; nine (09) IGS stations and one (01) Algerian station, while the network in the high-latitude region contains eight (08) IGS stations (see figure 1 and table 1). Both networks share the same observation period; from day 204 to 218 of the year 2023 (i.e. from July 23 to August 6, 2023).

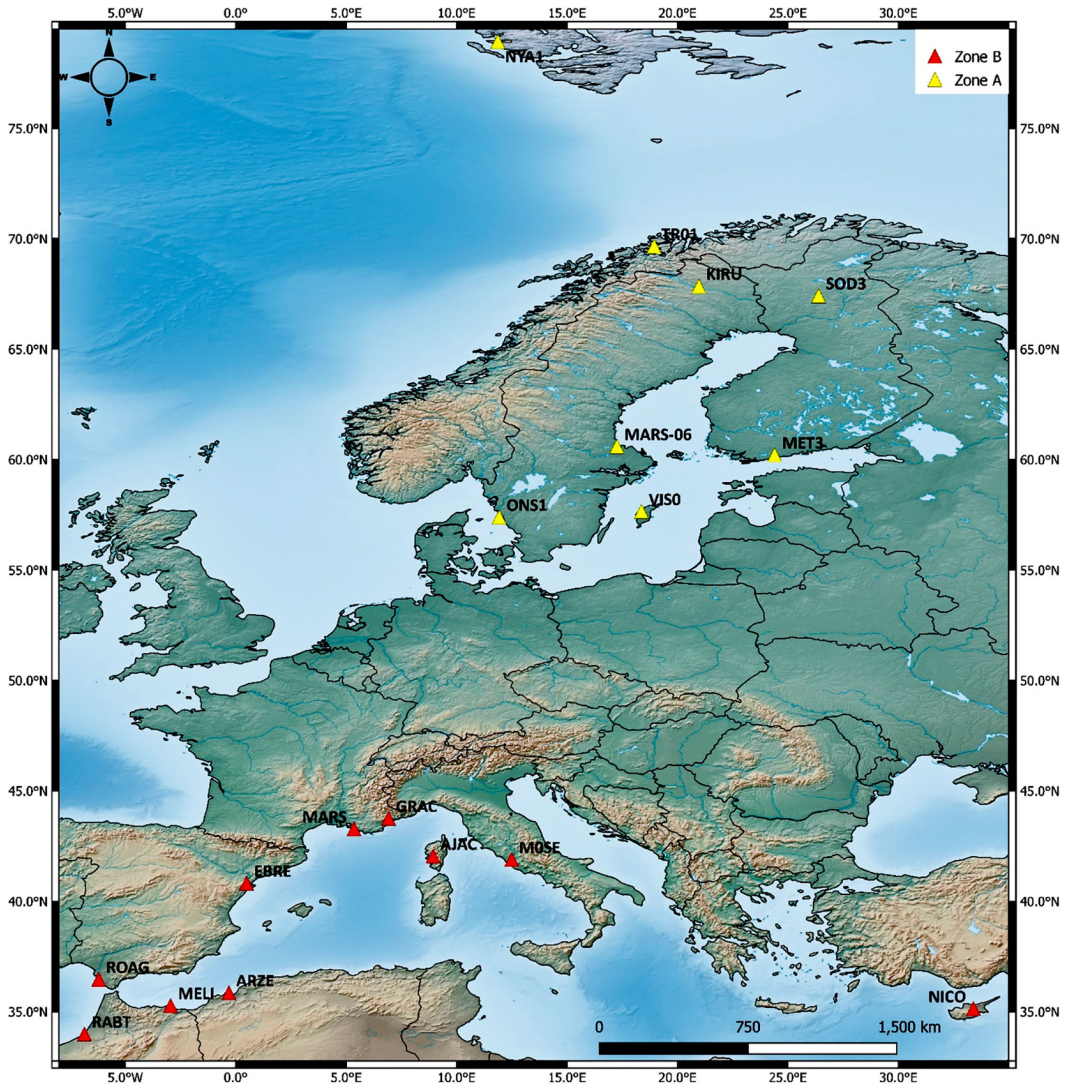

Figure 1: Geographic location of the used GNSS stations.

Table 1: Characteristics of the used GNSS stations

Zone	Station	Latitude (°)	Longitude (°)	Antenna type	Receiver type
Zone A: High- latitude region	**KIRU** KIRU00SWE	67.857	20.968	SEPCHOKE_B3E6 - SPKE	SEPT POLARX5TR
	MARS-06 MAR600SWE	60.595	17.259	JAVRINGANT_DM - OSOD	SEPT POLARX5
	MET3 MET300FIN	60.217	24.395	JAVRINGANT_DM - SCIS	JAVAD TRE_3 DELTA
	NYA1 NYA100NOR	78.93	11.865	ASH701073.1 - SNOW	TRIMBLE NETR9

Zone	Station	Latitude (°)	Longitude (°)	Antenna type	Receiver type
Zone A: High- latitude region	**ONS1** ONS100SWE	57.395	11.925	LEIAR25.R3 - LEIT	TRIMBLE ALLOY
	SOD3 SOD300FIN	67.421	26.389	JAVRINGANT_DM - SCIS	JAVAD TRE_3 DELTA
	TR01 TRO100NOR	69.663	18.94	TRM59800.00 - SCIS	TRIMBLE NETR9
	VIS0 VIS000SWE	57.654	18.367	AOAD/M_T - OSOD	SEPT POLARX5
Zone B: Mediterranean mid-latitude region	**ARZE**	35.851	-0.302	TRM57971.00 - NONE	Trimble Net R9
	AJAC AJAC00FRA	41.927	8.763	TRM115000.00 - NONE	LEICA GR50
	EBRE EBRE00ESP	40.821	0.492	LEIAR25.R4 - NONE	LEICA GR50
	GRA GRAC00FRA	43.754	6.921	TRM57971.00 - NONE	LEICA GR50
	M0SE M0SE00ITA	41.893	12.493	LEIAR25.R4 - LEIT	LEICA GR50
	MAR MARS00FRA	43.279	5.354	TRM57971.00 - NONE	LEICA GR50
	MELI MELI00ESP	35.281	-2.952	LEIAR25.R4 - LEIT	LEICA GR50
	NICO	35.141	33.396	LEIAR25.R4 - LEIT	LEICA GR50
	RABT RABT00MAR	33.998	-6.854	TRM29659.00 - SCIS	JAVADTRE_3 DELTA
	ROAG ROAG00ESP	36.463	-6.206	LEIAR25.R4 - NONE	SEPT POLARX5TR

4.2 Methodology

The methodological framework adopted in this study is structured into two main experimental phases: (i) assessment of tropospheric mapping functions performance under varying elevation cut-off angles, and (ii) evaluation of the combined use of different mapping functions with ATML corrections on the consistency of GNSS solution results.

The complete research workflow, encompassing initial data processing and both experimental phases, is comprehensively summarized in Figure 2. Each step is described in detail below to provide a thorough understanding of the procedures implemented.

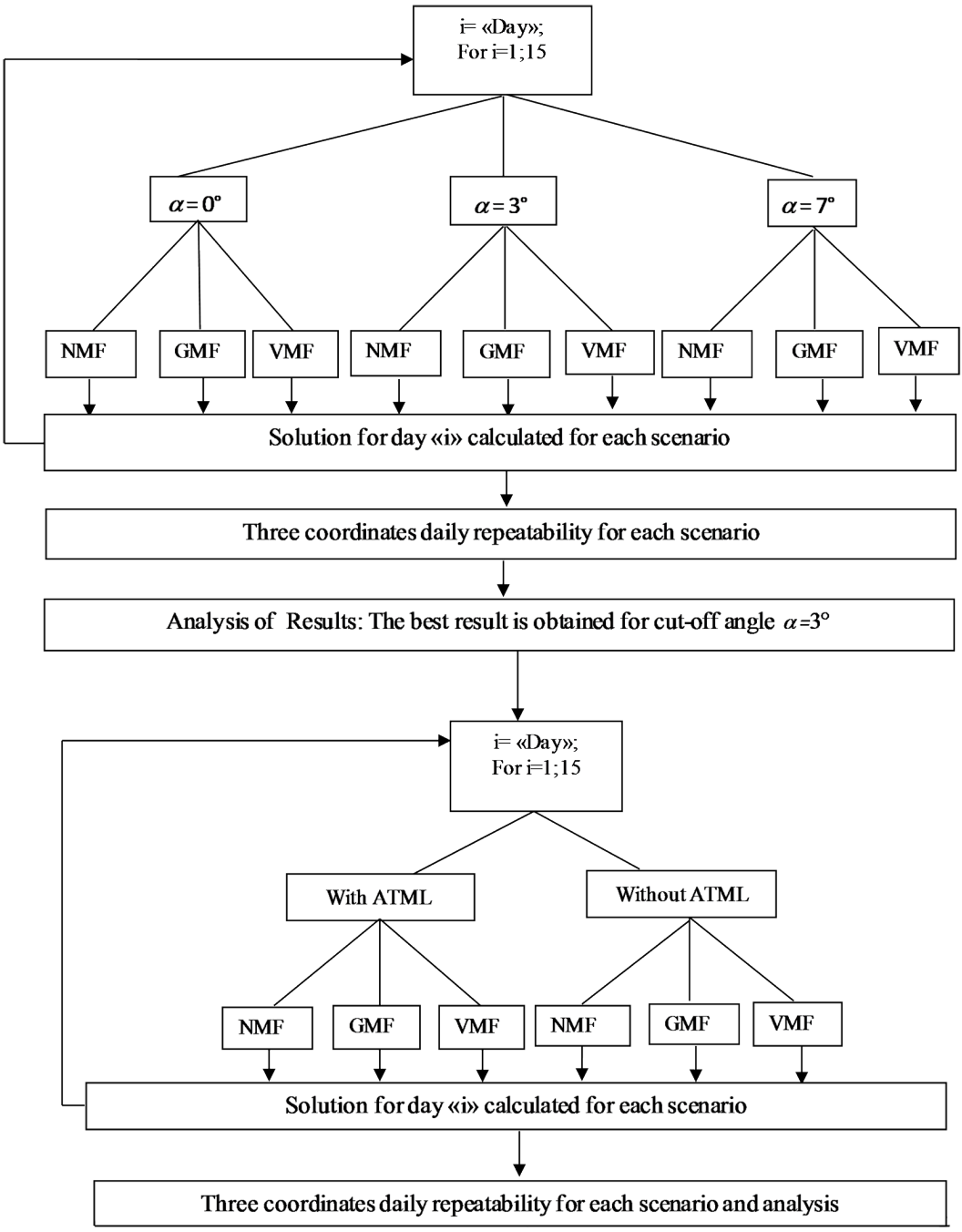

Figure 2: Methodology used in the research.

4.2.1 Evaluation of tropospheric mapping functions under different elevation cut-off angles

This initial experimental phase systematically assessed the impact of various elevation cut-off angles on the performance of different tropospheric mapping functions. This comprehensive evaluation is outlined in the upper part of Figure 2, aiming to identify the optimal configuration for subsequent processing.

Specifically, we investigated three cut-off angles (0°, 3°, and 7°) in combination with three widely used mapping functions: VMF1, GMF, and NMF. For each scenario, defined by a unique combination of a cut-off angle and a mapping function, 15 days of GNSS data were processed. The daily repeatability of the three coordinates (North, East, Up) was computed for each scenario, serving as the primary performance metric to assess solution stability and accuracy. The analysis of these results, as depicted in the first part of Figure 2, consistently demonstrated that the optimal performance was obtained with a cut-off angle of 3°.

4.2.2 Impact of the combined use of ATML with the mapping functions

Following the initial optimization phase, the second key objective of this study was to assess the specific impact of ATML on the consistency of GNSS solution results. This section details the methodology employed to integrate ATML corrections considering three different mapping functions (VMF1, GMF and NMF) into our processing workflow and to quantify their effect on solution repeatability, building upon the optimal configuration identified in the preceding phase. This approach is comprehensively illustrated in the lower part of Figure 2.

In this phase, the optimal configuration from the previous phase (3° elevation cut-off angle) is employed. This approach was chosen to isolate the distinct impact of specific combinations of ATML corrections with mapping functions, thus guaranteeing that any observed improvements can be directly linked to the effective pairing of ATML corrections with mapping functions.

This methodology is applied on two GNSS networks located in two different latitude zones (the Mediterranean mid-latitude and the high-latitude zones). For each zone, all three mapping functions (NMF, GMF, and VMF1) were tested with and without the ATML modelling. This allowed for a direct comparison of the performance of each mapping function under different situations, providing a clear assessment of ATML's contribution.

After computing the solutions for each scenario, the daily repeatability of the three coordinates (North, East, Up) was analysed. Repeatability served as a robust indicator for evaluating the consistency and precision of GNSS solutions under various ATML correction strategies.

4.2.3 GNSS data processing

All GNSS data were analysed using the GAMIT/GLOBK software, developed at the Massachusetts Institute of Technology (MIT). Data are processed in 24-hour sessions (from 00:00 to 23:59 UTC) to average out errors such as the effect of day/night alternation on the troposphere and ionosphere, and the effect of geometric variation in the satellite constellation (Leick et al., 2015; Herring et al., 2018). The satellite orbits used in the analysis are the final combined products provided by IGS. Several corrections and models were applied during the processing:

Geometric Offset: The software accounts for the geometric offset between the antenna's position and the satellite's center of mass.

Earth Rotation: Variations in Earth rotation are modelled using parameters provided by the International Earth Rotation and Reference Systems service (IERS).

Tidal Effects: Both lunisolar and polar solid Earth tides are considered. The elastic response to ocean tides is modelled using the FES2004 tidal model.

Ionosphere effect: The Ionosphere-Free combination is used to eliminate the ionospheric effect.

Troposphere modelling: Accurate modelling of tropospheric delay is a key factor influencing GNSS signal accuracy.

For the ZHD, we employed the Saastamoinen a priori model, as implemented in GAMIT, combined with the GPT2 meteorological model to provide pressure, temperature, and humidity parameters. This step corrects for the predictable, pressure-dependent portion of the delay.

The ZWD was estimated with position coordinates and ambiguities. The Piece-Wise Linear (PWL) method, offered by GAMIT, was chosen for ZWD estimation to capture the high spatiotemporal variability of the troposphere, with values estimated hourly to ensure temporal resolution consistent with tropospheric dynamics.

Horizontal gradients, both east west and north-south components were estimated at 2-hours per day. This resolution was selected to better model the azimuthal asymmetry in tropospheric conditions, particularly relevant for precise GNSS applications.

5 TESTS AND RESULTS

5.1 Impact of ZTD Estimation

This section presents the results quantifying the impact of ZTD parameter estimation on GNSS positioning repeatability. Two distinct strategies were compared: one where only the a priori Saastamoinen model was applied (Case 1: Without Estimation), and another where ZTD parameters were estimated every 2 hours along with horizontal tropospheric gradients, utilising the VMF1 mapping function (Case 2: With Estimation). The statistical analysis relies on daily repeatability, quantified by the Weighted Root Mean Square (WRMS), defined in equation 14.

$$WRMS_y = \sqrt{\frac{\frac{n}{n-1}\sum_{i=1}^{n}\frac{\left(y_i - y\right)^2}{\sigma_i^2}}{\sum_{i=1}^{n}\frac{1}{\sigma_i^2}}} \tag{14}$$

Table 2 summarizes the WRMS values for the East, North, and Up coordinate components for each station, comparing the two processing cases. The results consistently demonstrate that the estimation of tropospheric parameters (Case 2) leads to a substantial improvement in the repeatability of daily solutions across all stations and components, compared to relying solely on the a priori model (Case 1). This improvement is particularly pronounced for the Up (height) component. For instance, stations like ARZE show a remarkable improve-

ment from 101.65 mm (without estimation) to 8.12 mm (with estimation), EBRE from 153.76 mm to 7.61 mm, and RABT from 84.12 mm to 7.63 mm. While not as pronounced as for the Up component, noticeable improvements are also observed for the East and North components. For example, for station ARZE, East repeatability improves from 23.1 mm to 1.73 mm, and North from 9.78 mm to 3.05 mm.

The results clearly show that the estimation of tropospheric parameters using mapping functions leads to a significant improvement in the repeatability of daily solutions, especially for the Up (height) component, where the repeatability improves, in some cases, from over than one meter to just a few millimetres.

Table 2: WRMS of three components in both cases: with and without ZTD estimation.

Station	None			VMF1		
	U (mm)	E (mm)	N (mm)	U (mm)	E (mm)	N (mm)
ARZE	101.65	23.1	9.78	8.12	1.73	3.05
AJAC	76.81	11.65	10.63	5.14	1.63	2.06
EBRE	153.76	23.17	3.42	7.61	2.63	4.22
GRAC	96.44	13.3	11.85	7.42	2.3	2.6
M0SE	37.16	5.52	12.56	2.73	1.03	1.45
MARS	120.24	19.3	9.53	9.12	1.85	2.99
MELI	41.91	25.93	11.95	4.14	0.97	2.48
NICO	46.45	29.95	13.53	5.27	1.32	3.38
RABT	84.12	28.99	20.03	7.63	1.78	3.15
ROAG	83.15	28.78	17.86	7.56	1.67	2.88

5.2 Impact of elevation cut-off angle

This section presents the results evaluating the impact of the elevation cut-off angle on the performance of the mapping functions, aiming to identify the optimum value for each function. As described in section 4.2.1, three analysis of cut-off angle impact per mapping function.

Figures 3, 4 and 5 illustrate the WRMS of the stations height component for NMF, GMF and VMF1 mapping function, respectively. We can see that:

For NMF, a 3° cut-off angle generally produced better repeatability than 7°. At station ARZE, the WRMS for 3° is 7.04 mm compared to 9.72 mm for 7°, representing a discrepancy of approximately 2.68 mm. Similar improvements are observed at stations like MARS (WRMS 6.34 mm at 3° vs 8.94 mm at 7°) and RABT (WRMS 6.43 mm at 3° vs 8.56 mm at 7°). The 0° angle consistently yields higher WRMS values across all stations.

The results for GMF show very similar repeatability performance between the 3° and 7° cut-off angles. For example, for station ARZE, the Up component WRMS is 7.27 mm at 3° and 7.25 mm at 7°, suggesting that a lower (3°) mask provides comparable performance to a higher one (7°) for this specific mapping function. The 0° angle again leads to degraded performance.

VMF1 demonstrated slightly better performance with a 7° cut-off angle compared to the 3° angle. For example, at station ARZE, the Up component WRMS is 7.18 mm at 7° compared to 7.26 mm at 3°. The 0° angle also shows inferior quality for VMF1.

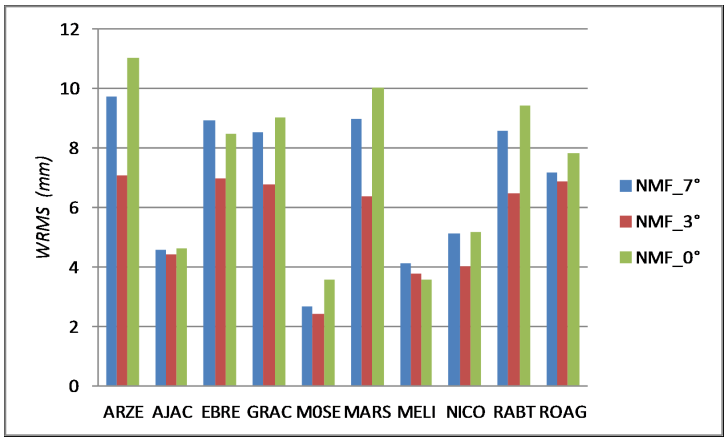

Figure 3: WRMS of vertical component in the case of NMF function and elevation cut-off angles of 0°, 3° and 7°.

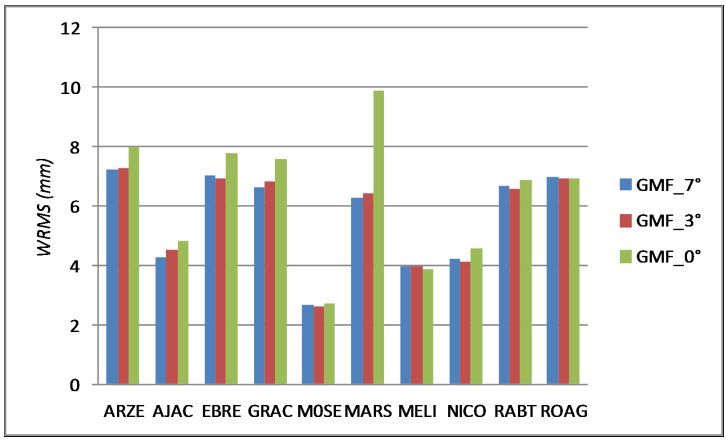

Figure 4: WRMS of vertical component in the case of GMF function and elevation cut-off angles of 0°, 3°and 7°.

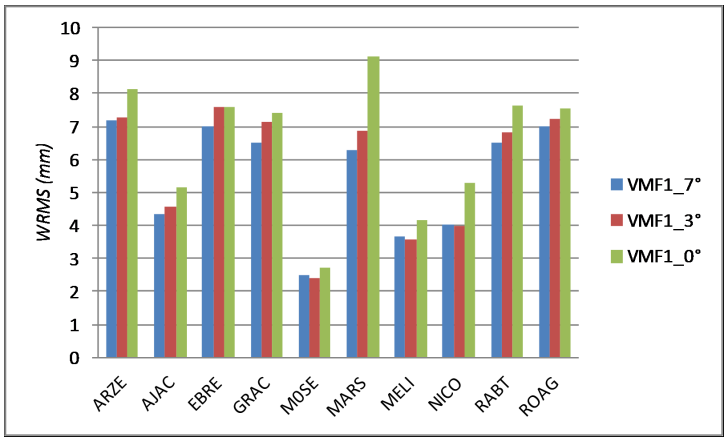

Figure 5: WRMS of vertical component in the case of VMF function and elevation cut-off angles of 0°, 3° and 7°.

5.3 Impact of mapping functions according to geographical area

To assess how mapping function performance varies with geographical location, we analysed data from two distinct regions: a network of ten GNSS stations in the Mediterranean and a second network comprising eight stations situated in a high-latitude area (see Figure 1). Basing on the previous results, an optimal cut-off angle of 3° was applied in this analysis. In this section, the ATML corrections were not applied.

Mediterranean Region

Table 3 summarises the WRMS values for the three components in the Mediterranean region relating to the GMF, NMF, and VMF1 mapping functions. The following observations can be made:

The repeatability of the solutions is consistently millimetric across all three mapping functions, demonstrating very stable and homogeneous performance. The discrepancies between them are sub-millimetric, indicating extremely similar results regardless of the function used in this region.

The analysis of the WRMS values clearly differentiates the performance across the Up component and the horizontal (North and East) components. As is typical in geodetic applications, the Up component exhibits significantly larger WRMS values for all mapping functions, reflecting its heightened sensitivity to atmospheric delays. WRMS values for Up component frequently exceed 4 mm and can reach over 7 mm (e.g., at ARZE), whereas horizontal components typically remain below 3 mm, except for EBRE station where the WRMS reaches a maximum of 4.26 mm. In most stations, GMF and NMF yield similar results, with slightly better repeatability for NMF. However, the VMF1 function provides lower quality results.

In contrast, the North and East components consistently show much smaller WRMS values, indicating higher precision in horizontal positioning especially for NMF and VMF1.

Table 3: Summary of WRMS of (N, E and U) components in the case of NMF, GMF and VMF1in Mediterranean region

Station	Component U (mm)			Component N (mm)			Component E (mm)		
	NMF	GMF	VMF1	NMF	GMF	VMF1	NMF	GMF	VMF1
ARZE	7.04	7.27	7.26	1.79	1.97	1.74	2.77	3.05	2.84
AJAC	4.4	4.53	4.57	1.45	1.52	1.51	1.87	2.03	1.9
EBRE	6.97	6.92	7.6	2.51	2.24	2.5	4.16	4.26	4.05
GRAC	6.74	6.85	7.13	1.98	2.02	2.04	2.17	2.16	2.33
MOSE	2.42	2.6	2.4	0.93	0.97	0.94	1.22	1.21	1.24
MARS	6.34	6.45	6.88	1.77	2.08	1.76	2.88	2.67	2.85
MELI	3.75	3.98	3.59	0.91	1.02	0.93	2.3	2.51	2.23
NICO	4.01	4.14	3.99	1.05	1.11	1.04	2.58	2.72	2.59
RABT	6.43	6.57	6.83	1.74	1.92	1.72	2.87	2.9	2.79
ROAG	6.83	6.92	7.25	1.64	1.75	1.56	2.63	2.79	2.67

High-Latitude Region

Table 4 presents the WRMS values for three components (Up, North, and East) in the high-latitude region. A detailed examination of this table reveals the following key observations:

The repeatability in the high-latitude network shows a wider range, from 1 mm to 12 mm across individual stations. In addition to this variability between stations, the repeatability derived from the use of the three mapping functions (NMF, GMF and VMF1) is slightly uneven in this region.

For the Up component, which is highly sensitive to atmospheric delays, GMF generally demonstrates strong performance in reducing WRMS values. Notably, GMF improved repeatability by about 30 % at TRO1 compared to NMF and VMF1.

In the horizontal (North and East) components, which inherently show higher precision, GMF frequently emerges as the standout performer with significant gains, except for NYA1 station where VMF1 provide better performance. For the North component, KIRU showed an exceptional 54.7% improvement with GMF over NMF and 65.81 % improvement over VMF1. Overall, GMF appears more effective at improving horizontal components.

Table 4: Summary of WRMS (N, E and U) components in the case of NMF, GMF and VMF1 functions in high latitude region.

Station	Component U (mm)			Component N (mm)			Component E (mm)		
	NMF	GMF	VMF1	NMF	GMF	VMF1	NMF	GMF	VMF1
KIRU	5.11	4.71	4.70	2.65	1.20	3.51	1.59	1.45	1.79
MAR6	0.83	0.73	0.78	0.48	0.49	0.52	0.75	0.64	0.73
MET3	11.15	10.8	10.43	1.17	1.25	1.27	1.67	1.56	1.92
NYA1	12.00	11.49	10.78	4.80	3.55	5.79	4.00	3.87	3.10
ONS1	1.10	0.82	0.89	1.15	0.84	1.07	0.80	0.73	0.82
SOD3	7.60	7.88	7.85	1.88	1.59	1.47	2.10	1.98	2.15
TRO1	1.60	1.13	1.67	2.21	1.59	2.67	0.80	0.65	0.72
VIS0	7.60	6.39	7.50	1.43	1.18	1.34	1.20	1.10	1.25

5.4 Impact of atmospheric pressure loading

This section presents the results evaluating the effect ATML corrections on GNSS solution repeatability. The analysis focuses exclusively on the Up component, as it is the most significantly affected by atmospheric loading effects. This assessment was performed by examining the repeatability of GNSS solutions processed with and without ATML corrections for each mapping function (GMF, NMF, VMF1), building upon the optimal configurations previously determined.

Figure 6 presents the WRMS values of the vertical component for three mapping functions—GMF, NMF, and VMF1—in the Mediterranean region, both with and without ATML correction. The results show that:

- For the VMF1 function, the repeatability indicated by the WRMS parameter showed a slight improvement after correcting for the ATML effects, particularly at the GRAC and RABT stations, where the WRMS values were respectively 7.11 mm and 6.85 mm without correction, and 6.35 mm and 5.9 mm after correction, which corresponds to an average improvement of 12%.
- For the GMF function, the correction for the ATML effect degrades the quality of the repeatability, especially at the ARZE, AJAC and ROAG stations where the WRMS values of 7.25 mm, 4.54, and 6.88 mm without correction were respectively increased to 8.0 mm, 5.2 and 7.65 mm after correction. This corresponds to a deterioration of 12%.

– For the NMF function, the use of ATML correction slightly degraded repeatability, particularly at the MARS, EBRE, and GRAC stations.
– The best configuration is VMF1 with ATML correction.

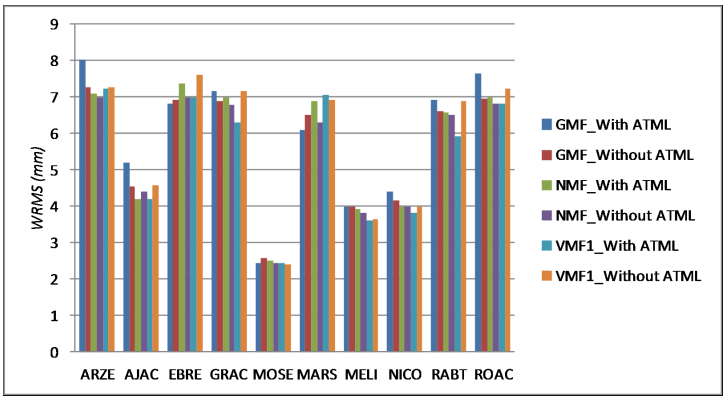

Figure 6: WRMS on the vertical component in the case of GMF, NMF and VMF1 with and without the ATML correction (Mediterranean region).

The same analysis was conducted for the network located in high latitude region. Figure 7 presents the WRMS of the vertical component for GMF, NMF and VMF1 with and without the ATML correction. We can see clearly that:

The application of ATML correction reduces WRMS for the majority of stations, demonstrating its role in stabilising GNSS solutions. Usually, when comparing mapping functions, VMF1 often show superior performance to NMF and GMF.

Stations MAR6, ONS1 and TRO1 stand out with inherently very good repeatability (WRMS around 0.8 mm), where differences between scenarios are minimal, but the favourable trend towards the use of ATML with VMF1 or GMF is maintained. The VMF1/ATML and GMF/ATML combinations generally offer the best performance, with slightly better results for VMF1/ATML.

Poor WRMS values (11-12 mm) at stations NYA1 and MET3 are a result of imprecise daily solutions, which in turn are caused by the low quality of the raw observations.

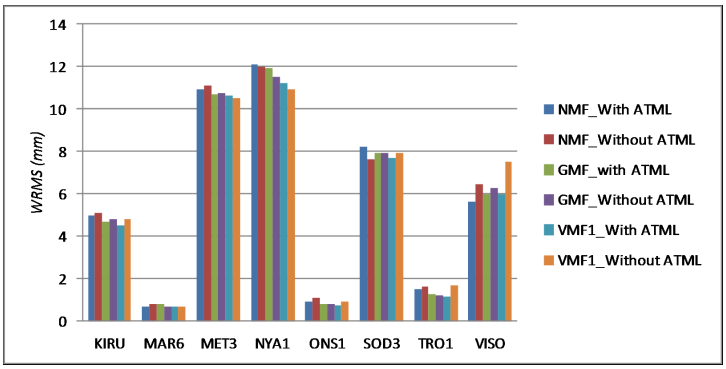

Figure 7: WRMS of the vertical component in the case of GMF, NMF and VMF1 with and without the ATML correction (High latitude region).

In summary, consistent with the earlier findings for the Mediterranean region, combining VMF1 with ATML correction proves to be a highly suitable option that enhances the accuracy of GNSS solutions. While its impact may not be significant across all stations or conditions, it however confirms its usefulness in high-precision geodetic applications.

6 CONCLUSION

This study investigated the impact of tropospheric modelling and atmospheric pressure loading on GNSS daily positions repeatability across two distinct geographical regions. The analysis, conducted using networks in Mediterranean and high-latitude environments, yielded several significant findings that advance our understanding of atmosphere modelling in high-precision GNSS applications.

The obtained results confirm the substantial benefits of estimating ZTD parameters in GNSS data processing. Estimating ZTD alongside horizontal gradients significantly improves the repeatability of daily GNSS positions, particularly for the Up component where errors can be reduced from over one meter to just a few millimetres. This gain underlines the limitations of relying solely on a priori models and emphasizes the necessity of tropospheric parameters estimation, especially in high-precision geodetic applications.

Moreover, the choice of elevation cut-off angle influences the repeatability of positions depending on the mapping function applied. A 3° cut-off angle generally provides better or equivalent results compared to 7°, while 0° systematically degrades performance, regardless of the used mapping function.

Geographical variability also influences mapping function performance. In the Mediterranean region, mapping functions yield nearly equivalent, millimetric-level performance, with slight advantages for NMF in vertical components and for VMF1 and NMF in horizontal ones. Conversely, in high-latitude regions, results vary more from station to station, with the GMF function proving to be the most effective for vertical and horizontal components in many cases, although some stations are exceptions and highlight the influence of local conditions and data quality. Nevertheless, incorporating ATML corrections proved beneficial, especially when used with the VMF1 mapping function. In the Mediterranean region, VMF1 combined with ATML correction provided up to 12% improvement in vertical repeatability, while GMF and NMF sometimes showed degraded performance under ATML corrections. In the high-latitude region, the inclusion of ATML corrections generally led to improved repeatability, with VMF1/ATML and GMF/ATML combinations yielding the most consistent enhancements, particularly at well-performing stations. The ATML corrections, particularly when combined with VMF1, yield the best overall performance, even though their impact may slightly vary depending on station-specific factors. This synergy confirms the importance of an integrated approach combining advanced mapping functions with atmospheric corrections, demonstrating that comprehensive tropospheric modelling requires consideration of multiple atmospheric effects simultaneously.

This analysis was based on specific time periods and seasonal conditions (15-day data analysis). Future studies should investigate the temporal stability of these findings across multiple years and varying seasonal conditions. Long-term analysis would provide insights into the consistency of optimal strategies and identify potential seasonal optimisation requirements. In addition, the superior performance of VMF1, which utilises numerical weather model data, suggests potential for further integration with high-resolution

meteorological models. Future research could explore the use of more sophisticated atmospheric models to enhance tropospheric delay modelling accuracy. Furthermore, as GNSS constellations continue to expand with systems like Galileo, BeiDou, and regional augmentation systems, future research should investigate how these tropospheric modelling strategies perform across different signal frequencies and constellation geometries. The increased observation redundancy may modify the preferences of optimal combinations of atmospheric modelling identified in this study.

References

Bevis, M., Businger, S., Chiswell, S., Herring, T., Anthes, R., Rocken, C., and Ware, R. (1994). GPS Meteorology: Mapping zenith wet delays onto precipitable water. Journal of Applied Meteorology, 33, 379-386.

Böhm, J., Niell, A., Tregoning P., Schuh, H. (2006a). Troposphere mapping functions for GPS and VLBI from European Centre for Medium-Range Weather Forecasts operational analysis data. J Geophys Res 111: B02406. DOI: https://doi.org/10.1029/2005JB003629.

Böhm, J., Niell, A., Tregoning, P., & Schuh, H. (2006b). Global Mapping Function (GMF): A new empirical mapping function based on numerical weather model data. Geophysical Research Letters, 33(7), L07304.

Böhm, J., Heinkelmann, R., and Schuh, H. (2007). Short note: a globalmodel of pressure and temperature for geodetic applications, Journal of Geodesy, 81, 679–683.

Böhm J., Schuh, H. (2013). Atmospheric Effects in Space Geodesy. Springer Atmospheric Sciences. Springer. ISBN 9783642369322.

Caiya, Y., Yamin, D., Changhui, X., Shouzhou, G., & Huayang, D. (2020). Effects and correction of Atmospheric pressure loading deformation on GNSS reference stations in Mainland China. Mathematical Problems in Engineering, 2020, 4013150. DOI: https://doi.org/10.1155/2020/4013150

Davis, J. L., Herring, T. A., Shapiro, I. I., Rogers, A. E. E., and Elgered, G. (1985). Geodesy by radio interferometry: effects of atmospheric modeling errors on estimates of baseline length. Radio Sciences., 20, 1593-1607.DOI : http://doi: 10.1029/RS020i006p01593.

Dach, R., Böhm, J., Lutz, S., Steigenberger, P., & Beutler, G. (2011). Evaluation of the Impact of Atmospheric Pressure Loading Modeling on GNSS Data Analysis. Journal of Geodesy, 85(2), 75–91. DOI: https://doi.org/10.1007/s00190-010-0417-z

El-Rabbany, A. (2002). Introduction to GPS: The Global Positioning System. Artech House, Boston, 176 p.

Fernandes, M. J., Lázaro, C., Ablain, M., & Pires, N. (2015). Improved wet path delays for all ESA and reference altimetric missions. RemoteSensing of Environment, 169, 50–74.

Fernandes, M. J., & Lázaro, C. (2016). GPD+ Wet tropospheric corrections for CryoSat-2 and GFO altimetry missions. Remote Sensing, 8(10), 851. DOI : https://doi.org/10.3390/rs8100851.

Herring, T. A., King, R. W., & McClusky, S. C. (2018). GAMIT Reference Manual: GPS Analysis at MIT – Release 10.7. Department of Earth, Atmospheric, and Planetary Sciences, Massachusetts Institute of Technology.

Hopfield, H. S. (1969). Two-quartic tropospheric refractivity profile for correcting satellite data. Journal of Geophysical Research, 74(18), 4487-4499.

Kos, T., Botinčan, M., Dlesk, A. (2009). Mitigating GNSS Positioning Errors due to Atmospheric Signal Delays. Pomorstvo. Journal of Maritime Studies, 23, 495-513.

Landskron, D., Böhm, J. (2018). VMF3/GPT3: refined discrete and empirical troposphere mapping functions. J Geod 92, 349–360. DOI : https://doi.org/10.1007/s00190-017-1066-2.

Leick, A., Rapoport, L., & Tatarnikov, D. (2015). GPS Satellite Surveying. (4th ed.). Hoboken, NJ: John Wiley & Sons. ISBN: 978-1-119-01849-1.

Luo, S. C. (2001). The model of evaluating precisions for atmospheric loading respond corrections, Geomatics and Information Science of Wuhan University. 3, 217–221.

Makabayi, B., Hunegnaw, A. (2015) Analysis of the accuracy of GMF, NMF, and VMF1 mapping functions with GPT 50 a priori zenith constraint in Tropospheric delay modelling, International Journal of Technoscience and Development, vol 2, Issue 1, Research Division of Technoscience Studies at Blekinge Institute of Technology.

Niell, A.E. (1996). Global mapping functions for the atmosphere delay at radio wavelengths,JGR, Vol. 101, No. B2, 3227-3246.

Namaoui, H. (2022). Evaluation of ERA5 reanalysis atmospheric water vapor variation in Algeria Geodetski Vestnik 66(03):403-411.

Petrov, L., Boy, J. P. (2004). Study of the atmospheric pressure loading signal in VLBI observations. Journal of Geophysical Research. DOI : https://doi.org/10.1029/2003JB002500

Rabbel, W. and Zschau, J. (1985). Static deformations and gravity changes at the earth's surface due to atmospheric loading, Journal of Geophysics. (1985) 56, no. 2, 81–89.

Saastamoinen, J. (1972). Atmospheric correction for the troposphere and stratosphere in radio ranging of satellites. In: Henriksen SW etal. (eds) The use of artificial satellites for geodesy, vol 15. AGU,Washington, 247–251.

Tesmer, V., Boehm, J., Heinkelmann, R. (2007). Effect of different tropospheric mapping functions on the TRF, CRF and position time-series estimated from VLBI. J Geod 81, 409–421.DOI: https://doi.org/10.1007/s00190-006-0126-9.

Thayer, D. (1974). An improved equation for the radio refractive index of air. Radio Sciences., 9, 803– 807.

Torres, B., Cachorro, V. E., Toledano, C., Ortiz de Galisteo, J. P., Berjón, A., de Frutos, A. M., Bennouna, Y., and Laulainen, N. (2010). Precipitable water vapor characterization in the Gulf of Cadiz region (southwestern Spain) based on Sun photometer, GPS, and radiosonde data. J. Geophys. Res., 115. DOI: https://doi.org 10.1029/2009JD012724.

Tregoning, P., van Dam, T.M. (2005). Atmospheric pressure loading corrections applied to GPS data at the observation level. Geophysical Research Letters 322(22). DOI: https://doi.org/10.1029/2005GL024104

Tuka, A, El-Mowafy, A. (2013). Performance evaluation of different troposphere delay models and mapping functions. Measurement 46(2):928–937.

DOI: http://dx.doi.org/10.1016/j.measurement.2012.10.015

Urquhart, L., Nievinski, F.G. & Santos, M.C. (2014). Assessment of troposphere mapping functions using three-dimensional ray-tracing. GPS Solut 18, 345–354 . DOI :https://doi.org/10.1007/s10291-013-0334-8

Van Malderen, R., and Coauthors. (2014). A multi-site intercomparison of integrated water vapour observations for climate change analysis. Atmospheric Measurement Techniques, 7, 2487—2512. DOI: https://doi.org 10.5194/amt-7-2487-2014.

van Dam, T.M., Blewitt, G., and Heflin, M. (1994). Detection of atmospheric pressure loading using the Global Positioning System, Journal of Geophysical Research. 99:23,939-23,950. DOI: https://doi.org/10.1029/94JB02122.

https://vmf.geo.tuwien.ac.at/trop_products/GNSS/VMF1/

Dekkiche H., Namaoui H., Bouaoula W., Bedjaoui Y, Bensttila K. (2025). Impact of tropospheric modelling and atmospheric pressure loading on GNSS position repeatability. Geodetski vestnik, 69 (4), 554-573.
DOI: https://doi.org/geodetski-vestnik.2025.04.554-573

Hicham Dekkiche
Algerian Space Agency, Center of space techniques
BP13, Arzew , Oran 31200
e-mail: hdekkiche@cts.asal.dz

Houaria Namaoui
Algerian Space Agency, Center of space techniques
BP13, Arzew ,Oran 31200
e-mail: hnamaoui@cts.asal.dz

Walid Bouaoula
Algerian Space Agency, Center of space techniques
BP13, Arzew ,Oran 31200
e-mail: wbouaoula@cts.asal.dz

Yasser Bedjaoui
Algerian Space Agency, Center of space techniques
BP13, Arzew ,Oran 31200
e-mail: yasserbedjaoui990@gmail.com

Karim Benstila
Algerian Space Agency, Center of space techniques
BP13, Arzew ,Oran 31200
e-mail: benskarim30@gmail.com